Nitrogen/Boron Doping Position Dependence of the Electronic Properties of a Triangular Graphene

Shansheng Yu, Weitao Zheng,* Chun Wang, and Qing Jiang

Department of Materials Science, Key Laboratory of Mobile Materials, MOE, and State Key Laboratory of Superhard Materials, Jilin University, Changchun 130012, People's Republic of China

ABSTRACT We investigate the effect of N/B doping on the electronic properties for a zero-dimensional zigzag-edged triangular graphene, wherein two sets of sublattices are unbalanced, using density functional theory (DFT). We find that the substitutional N/B atom energetically prefers to distribute in the major sublattice. After the N/B doping, the net spin for triangular graphene is reduced and full or partial depolarization occurs depending on doping sites. Our DFT calculations show that the triangular graphene with N/B doped in the major sublattice has a larger energy gap, and the electronic properties depend on the doping position. There is an impurity state below or above the Fermi level for the N/B-doped triangular graphene, depending on the sublattice at which the dopant locates. The dependence of the electronic properties on doping position is attributed to the competition between the Coulomb attraction of N^+ (B^-) and the correlation with nonbonding states for the extra charge introduced by the N/B atom.

KEYWORDS: graphene · electronic structures · density functional theory · nanoelectronics · doping

Graphene, a natural realization of two-dimensional carbon crystal, has been intensively investigated for its interesting physical properties and potential technological applications,[1−13] and these peculiar properties such as massless high mobility,[1] quasi-particles,[2] and quantum Hall effect[4,9] make it different from conventional materials. Further electron confinement and some graphene nanostructures, such as one-dimensional graphene nanoribbons (GNRs) and zero-dimensional graphene quantum dots (GQDs), have also attracted interest, which can provide a possibility to explore low-dimensional transport and perspective for carbon-based nanoelectronics. Progress in preparing GNRs[12,14−16] and GQDs[4,11,13] has been reported, which are top-down or bottom-up approaches. For instance, some GQDs have already been manufactured by soft-landing mass spectrometry,[5] and recently, graphene nanoislands have also been epitaxially grown on 6H-SiC(0001).[17]

The electronic properties of graphene nanostructures have widely been investigated. Tight-binding approximation calculations[18−21] predict that one-dimensional GNRs with armchair-shaped edges can be either metallic or semiconducting, depending on their widths, while those with zigzag-shaped edges are metallic with two flat bands at the Fermi energy. First-principles calculations show that GNRs with hydrogen passivated edges always have nonzero and direct energy gaps.[22,23] The energy gaps of GNRs with armchair-shaped edges originate from edge quantum entrapment, while the gaps for GNRs with zigzag-shaped edges arise from a staggered sublattice potential due to spin ordered states at the edges.[23−25] First-principles calculations have also been performed to investigate the electronic properties for finite length GNRs, *viz.*, rectangular-shaped graphene,[26−28] and the calculated results reveal that, in addition to edge quantum entrapment from ribbon width, finite size effects along the ribbon length affect the electronic states drastically. For finite length GNRs, there are no zero-energy states in comparison with infinite length GNRs.[29] Very recently, several theoretical calculations have been carried out to study the electronic properties and magnetism for other shaped zero-dimensional GQDs.[29−35] In particular, only triangular GQDs with zigzag edges have degenerate zero-energy states and show metallic ferromagnetism, in which the net spin increases linearly with its size, which is quite different from that for GNRs, being zero regardless of its size and edge type. It also has been predicted that the net magnetic moments in triangular GQDs are usually satisfied with Lieb's theorem.[36] In addition, the energy gaps for GQDs in the graphane can be controlled by the size.[37] These special properties render

*Address correspondence to wtzheng@jlu.edu.cn.

Received for review September 11, 2010 and accepted November 15, 2010.

Published online November 19, 2010. 10.1021/nn102369r

GQD as the building block for nanodevices such as spin memory, transistors, solid-state qubits, and perhaps optoelectronics applications.[31,38,39]

In order to enrich the potential applications, the doping of other elements into graphene nanostructures is the efficient way to tune the electronic structures. It is well-known that the N/B atom is a general dopant within the carbon materials, which is a neighbor to the C atom in the periodic table. Various techniques have been employed to incorporate N or B atoms into carbon materials.[40−46] Alternatively, an atom-by-atom substitution technique using a scanning tunneling microscope can be realized to control nanostructures accurately.[47] N/B dopant can inject electron/hole into carbon-based materials, thus changing the electronic and transport properties.[48,49] Theoretically and experimentally, the N/B-doped carbon-based materials are widely investigated.[50] Using density functional theory (DFT), we have investigated the electronic properties for N/B-doped carbon nanotubes (CNTs) and GNRs.[49] For N-doped GNRs with zigzag edges, we have first found that the site of impurity energy level introduced by the N atom is related to the competition between the Coulomb interaction and correlation with charges.[51] Our calculated results suggest that the electronic properties of N-doped GNRs can be controlled by adjusting the doping sites. It should be emphasized that, different from zigzag GNR with a total spin of zero, the zero-dimensional triangular GQD with zigzag edges has a finite total spin. Hence, it can be expected that both the electric and magnetic properties of triangular zigzag GQD can also be affected by the N/B dopant, and they may be different from zigzag GNRs. In this work, we aim to investigate the electronic properties for N/B-doped triangular GQDs with hydrogen passivated zigzag edges using DFT calculation and try to explore how N/B doping influences the electronic properties of GQDs.

RESULTS AND DISCUSSION

The structure of a selected triangular GQD with hydrogen passivated zigzag edges is shown in Figure 1. Its edge size was $n = 6$, which consisted of 61 carbon atoms and 21 hydrogen atoms, wherein the hexagonal lattice of graphene contained two sets of sublattices, denoted as A and B, respectively. In the triangular GQD, the three edges belong to the same sublatice, hereafter A. Hence, a triangular GQD did not contain the same atoms in each sublattice, namely $N_A \neq N_B$, and in this work, the number of atoms in different sublattices satisfied $N_A - N_B = n - 1 = 5$. The N/B-doped GQD was modeled by direct substituting of one carbon atom by one N/B atom in the hexagonal lattice, which could lead to different doping positions. The letters in Figure 1 denote the different doping positions of the substitutional N/B atom, and 14 different configurations for doped GQDs were considered in this work.

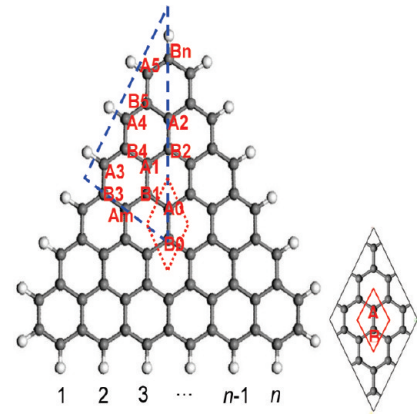

Figure 1. Schematic structure of a zigzag-edged triangular GQD with edge size $n = 6$, wherein the letters denote the different doping positions, and A and B represent the two subsets in the hexagonal lattice for graphene, as shown in the inset. The white and gray balls denote the hydrogen and carbon atoms, respectively.

Pristine Triangular Graphene. First, we have performed the spin-unpolarized DFT calculations on the electronic structure for a pristine zigzag-edged triangular GQD with edge size $n = 6$, and the energy spectrum and the density of states (DOS) are shown in Figure 2a,b, respectively. The half-filled states near the Fermi level are zero-energy states which are called nonbonding states (NBSs), and the existence of these degenerate NBSs is the same as from the TB calculated results.[29,30] Like GNR, the topology constraint gives rise to these sharp NBSs near the Fermi level, which come from the edge trapping of the bonding electrons and π-electron polarization.[25] These half-filled NBSs are not stable and can imply possible magnetic states when the degree of freedom for spin is unrestricted, and hence the spin-polarized DFT has to be employed in this work. The energy difference between spin-polarized and spin-unpolarized states is 0.47 eV and in favor of the polarized state. Figure 2c,d shows that a split for the degenerate NBSs and an energy gap of 0.59 eV appears near the Fermi level when the degree of freedom for spin is unrestricted, comparable to other theoretical results,[31] which indicates that it is possible to measure the magnetic moment at room temperature. Five NBSs with the same spin orientation (assigned as spin up) are occupied, and the total spin for pristine GQD satisfies $2S = N_A - N_B = n - 1 = 5$, in agreement with Lieb's theorem.[36] These results are consistent with those predicted by mean-field approximation[30] and DFT calculations with local density approximation.[31]

We have further calculated the spatial distribution of NBSs near the Fermi level for pristine GQD with edge size $n = 6$. The highest occupied molecular orbital (HOMO) and HOMO-1 are degenerate states, and the sum of the electronic distribution for these two orbitals is shown in Figure 3a, wherein the orbitals are extended in the GQD. The lowest unoccupied molecular orbital (LUMO) and LUMO+1 are also degenerate ex-

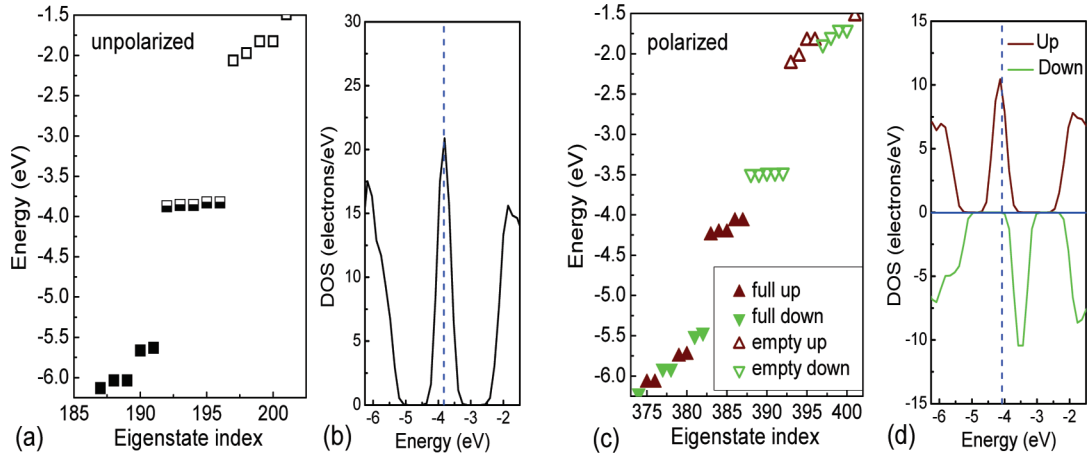

Figure 2. Calculated self-consistent energy spectra and DOS for a pristine GQD with edge size $n = 6$ using spin-unpolarized DFT (a,b) and spin-polarized DFT (c,d). Full, empty, and half-filled symbols correspond to full, empty, and half-filled states, respectively. The Fermi level is labeled by a dashed line.

tended orbitals in Figure 3b, while the other nonbonding orbitals distribute mainly near the zigzag edges, as shown in Figure 3c,d. The distribution of NBSs near the zigzag edges is denser than that in the inner area. For some graphene nanostructures, such as armchair-edged triangular GQDs, hexagonal GQDs, and rectangular GQDs,[29,30] the numbers of two sublattices are the same ($N_A = N_B$), where there are no NBSs near the Fermi level. However, in the zigzag-edged triangular and trapezoid GQDs,[34] the NBSs come into existence, and the number of NBSs equals the difference between two sublattices ($N_A - N_B$), hence NBSs originate from the unbalanced sublattice. Figure 3 exhibits that all of the NBSs distribute only in the major sublattice (sublattice A) for pristine GQD. Furthermore, the occupied NBSs are all of the spin-up orbitals near the Fermi level in Figure 2. Due to the asymmetry in spatial distribution, the remaining spin-up orbitals are attracted to the sublattice A by the exchange interaction while the spin-down orbitals are repelled from the sublattice A and attracted to the sublattice B.[31] The calculated spin density difference for pristine GQD is shown in Figure 3e, in which the spin-up orbitals distribute exclusively in sublattice A and mainly at the zigzag edges, which is consistent with the distribution of NBSs. The whole system develops a ferrimagnetic order with opposite spins on the subsets of the sites and with the total spin-up larger in the sublattice A than the total spin-down in the sublattice B. The value of total net spin $S = N_A - N_B = (n - 1)/2$ increases linearly with the size of GQD.[31]

N/B-Doped Graphene Quantum Dots. We have selected 14 different doping positions in the zigzag triangular GQD with size $n = 6$, as shown in Figure 1. The doping positions A0∼A5 and Am lie in the sublattice A, while B0∼B5 and Bn are located in the sublattice B. In our work, the considered configurations for N-doped GQDs are denoted by N-A0∼N-A5, N-Am, N-B0∼N-B5, and N-Bn, while for B-doped GQDs, those cases are labeled by B-A0∼B-A5, B-Am, B-B0∼B-B5, and B-Bn, respectively. The corresponding total energy differences for these N/B-doped GQDs are given in Table 1 and are also plotted in Figure 4. The zigzag edge of triangular GQDs breaks the symmetry between the two sublattices of the honeycomb lattice, behaving like a defect. Therefore, the N/B dopant more energetically prefers to lie at the edge than that it does in the inner area, which is in good agreement with our previous work on N/B-doped GNRs.[51,52] It is worth emphasizing that we find that the substitutional N/B atom energetically prefers to distribute in the major sublattice for GQD, and the most favorable doping position locates at A3, namely, the middle

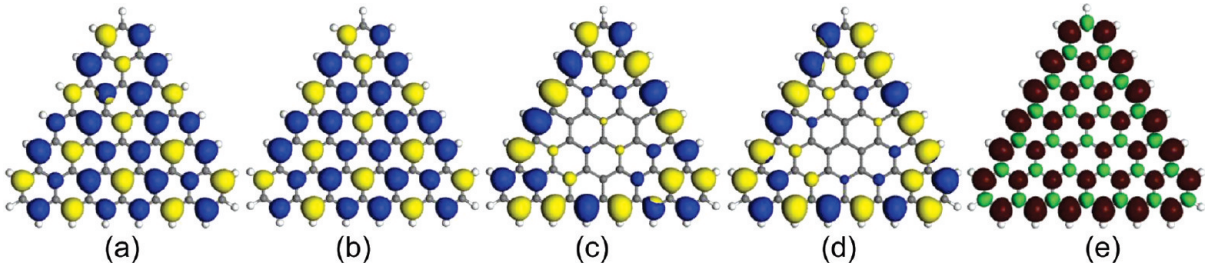

Figure 3. Sum of electronic distribution for (a) HOMO and HOMO-1, (b) LUMO and LUMO+1, (c) HOMO-2, HOMO-3, HOMO-4, and (d) LUMO+2, LUMO+3, LUMO+4 in pristine GQD with size $n = 6$, where the blue and yellow shapes denote positive and negative wave function contours, respectively, and the isosurface value is ±0.02 electrons/au^3. (e) Isosurface spin density difference for pristine $n = 6$ GQD, in which wine and green correspond to up and down spins, respectively. Spin density difference contour is shown at the value of 0.01 electrons/au^3.

TABLE 1. Relative Total Energy (ΔE), Net Total Spin Value (S), and Energy Gaps (E_{gap}) for the N/B-Doped and Pristine (P) GQDs[a]

	P	N-A0	N-Am	N-A1	N-A2	N-A3	N-A4	N-A5	N-B0	N-B1	N-B2	N-B3	N-B4	N-B5	N-Bn
ΔE		0	−0.11	−0.09	−0.13	−1.05	−1.03	−0.88	0.42	0.37	0.31	0.11	0.14	0.13	−0.19
S	2.5	2	0	0	0	0	0	0	0	0	1	−1	0	0	0
E_{gap}	0.59	0.27	0.27	0.22	0.06	0.29	0.30	0.29	0.21	0.15	0.12	0.25	0.22	0.21	0.29

	P	B-A0	B-Am	B-A1	B-A2	B-A3	B-A4	B-A5	B-B0	B-B1	B-B2	B-B3	B-B4	B-B5	B-Bn
ΔE		0	−0.34	−0.19	−0.14	−0.61	−0.54	−0.3	0.23	0.29	0.34	−0.02	0.08	0.08	0.52
S	2.5	0	2	0	0	0	0	0	2	0	0	2	0	−1	0
E_{gap}	0.59	0.27	0.44	0.31	0.20	0.29	0.27	0.29	0	0.24	0.19	0.14	0.22	0.28	0.29

[a]The unit of ΔE and E_{gap} is eV. For N/B-doped GQDs, ΔE is relative to the total energy of N/B-A0.

of the zigzag edge. It is consistent with the electronic distribution near the Fermi level in Figure 3.

When the dopant lies at A3 or A0, the bond lengths near the dopant are shown in Figure 5. It is clearly exhibited that the bonds adjacent to dopant are changed. For N doping, the N−H and N−C bonds are contracted, while the B−H and B−C bonds are stretched for B doping. The local structural distortion induced by N doping is very small, whereas that by B doping is more pronounced. Hence, the distribution of NBSs is the main factor, which determines that the N dopant prefers to lie at the edge, in which the density at the edge is denser than that in the inner area. For the B dopant, electron-deficient substitution likely forms "in-plane" bonding configurations. When the distance between the B dopant and the edge is shorter, the structural distortion of doped GQD is more prominent. It seems that the B dopant prefers to locate in the inner region. However, the existence of NBS distribution is noted. Consequently, combining these two facts, the edge appears to be a more energetically favorable site for the B dopant, and the energy differences between doping at the edge and doping in the inner are are clearly smaller than those for N-doped GQDs. It is noted that the configuration N-Bn is more favorable than other cases such as N-Bx (x = 0−5). This behavior is related to the site of Bn lying at the angle of the triangular GQD, which can lead to formation of N−H. The H−N bond is more stable than that of C−N. However, B-Bn is energetically unlikely in comparison with other cases such as B-Bx (x = 0−5) owing to large local structural distortion induced by B doping, where the H atom adjacent to B moves outward from its original position by 0.12 Å. Note that this stretch of the B−H bond is so large that it is accompanied by symmetry breaking.[52]

The electronic properties for N/B-doped GQDs have been calculated, and the calculated electronic energy gaps (HOMO−LUMO) for different configurations are listed in Table 1, from which we find that the energy gaps for all N/B-doped GQDs are smaller than that for pristine GQD (0.59 eV). Furthermore, the energy gap also depends on the doping position, and the GQD with N doped at the zigzag edge has a relative large energy gap in comparison to the case with N doped in the inner region. In addition, the gap for GQD with N/B doped at sublattice A is slightly larger than that with N/B doped at sublattice B, except for the doping position A2. The N/B dopant at some sublattice creates a larger energy gap than 0.2 eV. It should be pointed out that we adopt the generalized gradient approximation (GGA) scheme which has a tendency to underestimate the energy gap. Therefore, the spin alignment may be stable at room temperature for some N/B-doped GQDs. When one extra electron is added, the magnetization of triangular GQD will collapse to the minimum possible value.[33] As an example, if a triangular GQD with n = 6 is charged by one electron, the total net spin will be 0,

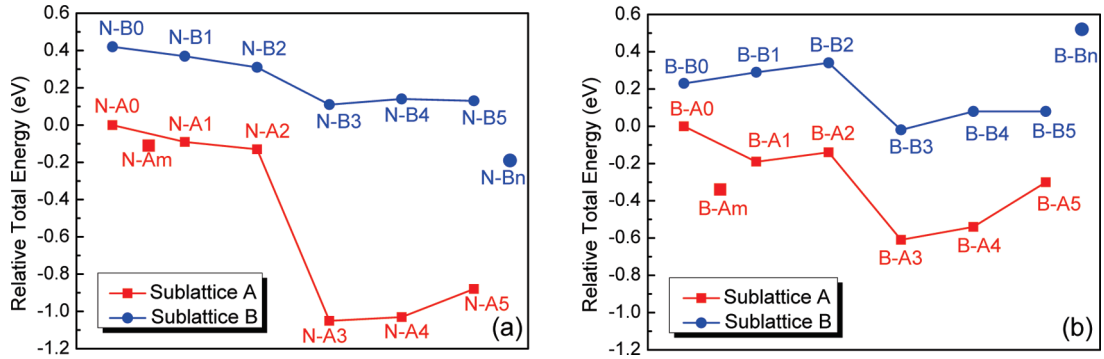

Figure 4. Relative total energies for N-doped (a) and B-doped (b) GQDs with different configurations. The solid lines are just guides for the eye.

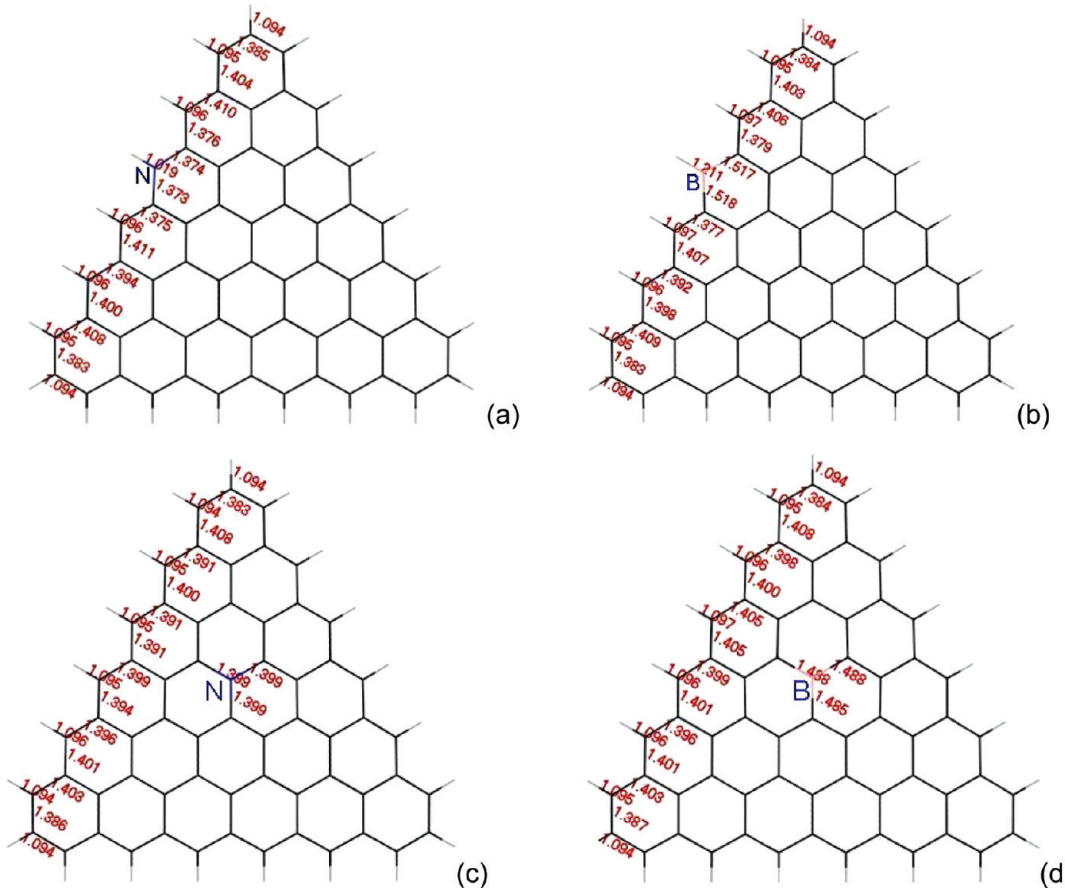

Figure 5. Bond lengths near the dopant and at the edge are shown when the N or B dopant lies at A3 (a,b) and A0 (c,d). The unit of bond length is Å.

viz., $S = 0$. Because the N atom has one extra electron in comparison with the C atom, for N-doped GQD, it is probable that the reduction of the net spin can take place. However, our results are different from above, as listed in Table 1, as the net spins for N-A0, N-B2, and N-B3 decrease to 2, 1, and -1 and for other configurations reduce to 0, which implies that these interesting variable magnetizations are also related to N^+. For B-doped GQDs, the extra charge is a positive hole introduced by the B dopant, and it is similar to N doping where magnetization of the doped GQD depends on the dopant doping site. The net spins for B-Am, B-B0, and N-B3 decrease to 2, B-B5 reduces to -1, and other configurations diminish to 0. It suggests that the spin polarization of GQD is fragile.

First, the calculated electronic structures for N-doped GQDs are shown in Figure 6. It is exhibited that the doping position plays an important role in the electronic structures. Compared to pristine GQD, it is visible that the full or partial depolarization occurs and electronic structures are altered largely for N-doped GQDs except for N-A0. For N-A0, the Fermi level is shifted upward and the band of down-spin NBSs is wider than that of pristine GQD. Furthermore, it is worth noting that the impurity energy levels designated by blue arrows distinctly come into existence below the Fermi level when N dopants lie at the zigzag edge of sublattice A, *viz.*, N-A3, N-A4, and N-A5. However, for GQDs with N doped in the inner area of sublattice B, namely, N-B0, N-B1, and N−B2, the clear impurity levels labeled by blue arrows appear above the Fermi level. Due to special position of N-Bn, there also exists an impurity level above the Fermi level. In order to explore the electronic structures of N-doped GQDs deeply, we have calculated their self-consistent energy spectra and corresponding electronic distribution of NBSs in Figure 7. It is found that there are six occupied and four unoccupied NBSs near the Fermi level, in which one orbital is occupied by the extra electron of the N dopant. It is clear that the N-A0 is a fully polarized state ($S = 2$), N-B2 and N-B3 are partially polarized ($S = 1, -1$), and other cases are fully depolarized states ($S = 0$). For the largest spin $S = 2$ case, the added electron simply occupies one spin-down orbital and other orbitals remain in their spin. Therefore, the electronic structure near the Fermi level for N-A0 is very similar to that for pristine GQD, except for the occupation of one spin-down orbital in N-A0. However, for other cases, the added electron induces the present electrons to be partially flipped in spin, which leads to a greatly modified electronic structure.

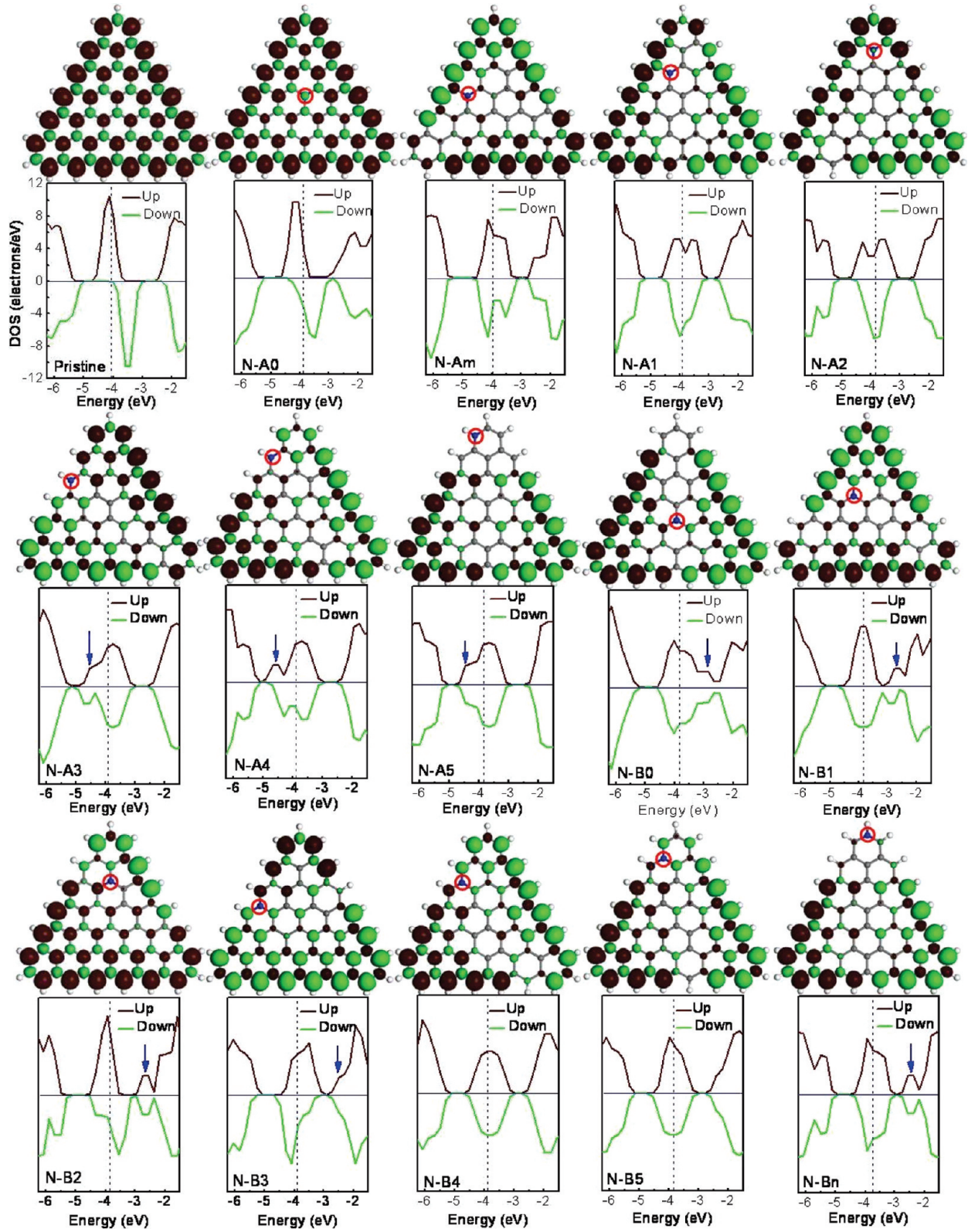

Figure 6. DOS and isosurface plots of spin density difference for N-doped GQDs with size $n = 6$, in which the Fermi level is labeled by a dashed line, and the site of the N dopant is marked by a red circle.

Moreover, it is worth noting that a complicated hybridization takes place after N doping. We have also observed that the special electronic states labeled by blue dashed arrows (circles) appeared in the occupied NBSs for GQDs with N doped in the sublattice A, which come from occupied NBSs. In contrast, for GQDs with N doped in the sublattice B, they exist above the unoccupied NBSs. The right insets in Figure 7 present that

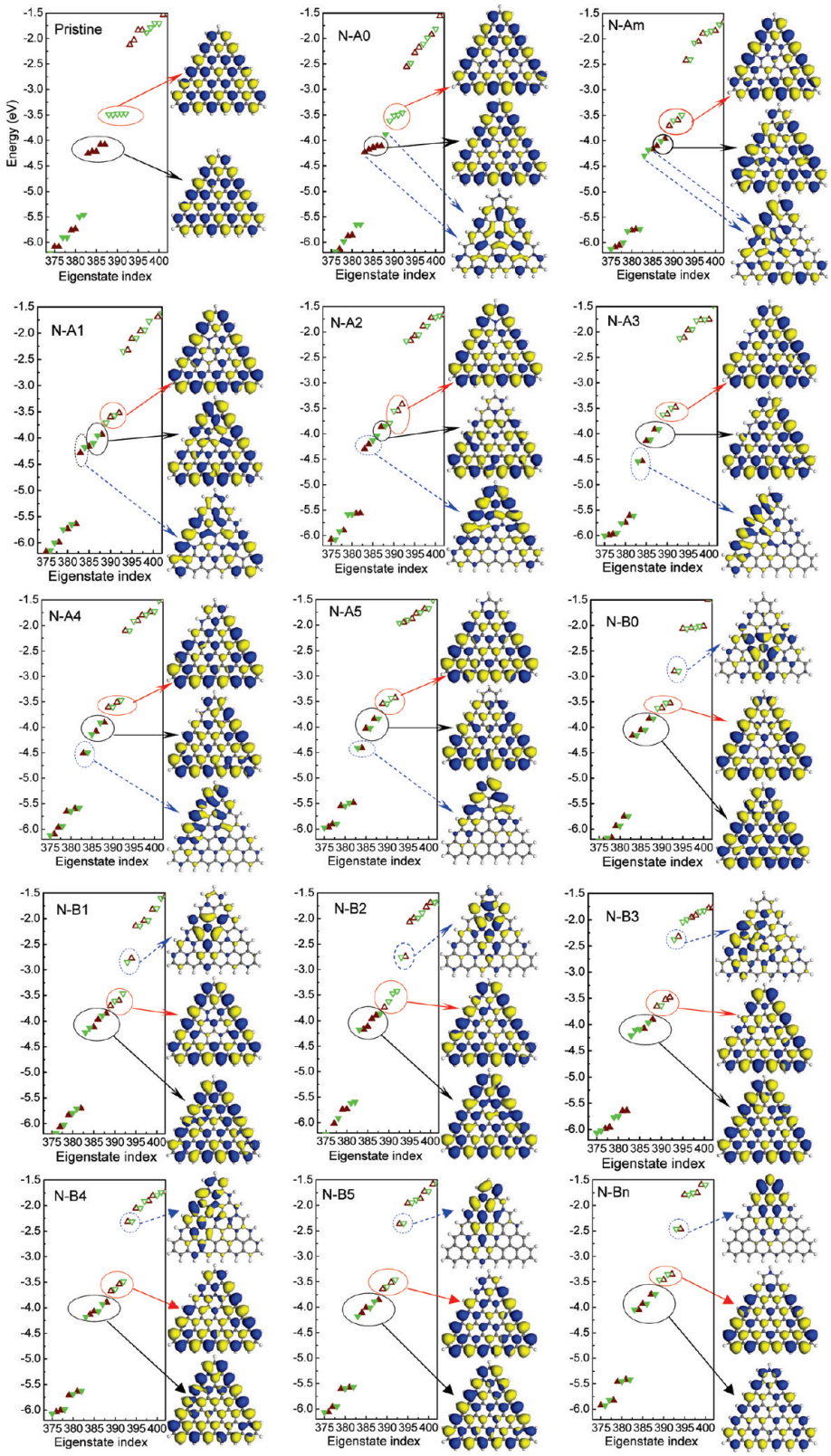

Figure 7. Calculated self-consistent energy spectra and NBS wave function isosurfaces for N-doped GQDs with size $n = 6$, in which full and empty symbols correspond to full and empty states, respectively. The upward triangle and downward triangle represent up and down spins, respectively. Occupied NBSs and unoccupied NBSs are denoted by black and red circles, respectively.

these electronic states are localized and concentrated around the N dopant site, where they exhibit antibonding states between C and N atoms owing to electron-sufficient N dopant. Due to no p orbtials of the H atom,

there are no electronic states between C and H atoms. It is clear that these striking nodal structures are similar to impurity states for N-doped GNRs and N-doped CNTs. Because these electronic states are introduced by the N dopant, they are also called impurity states, which correspond with impurity energy levels in DOS. Hence, although the impurity energy levels for some GQDs are not shown in Figure 6, their positions can be obtained through their corresponding self-consistent energy spectra in Figure 7. For example, for N-B3, through its energy spectrum, we can find out the site of impurity energy level shown by a blue arrow in Figure 6. All other NBSs retain the features in pristine GQD (*i.e.*, distribute exclusively in sublattice A, and extended or localized at the zigzag edge), as shown on the right insets in Figure 7.

What is the formation mechanism of the impurity states, and how does it depend on the doping sublattice? Similar to N-doped infinite GNRs in our previous work,[51] for N-doped triangular GQDs, the competition between the Coulomb interaction and correlation with charges also determines position of the impurity energy level. When an additional electron is added in triangular GQDs, it primarily occupies the unoccupied nonbonding orbital which distributes exclusively in sublattice A due to the unbalanced sublattice. This feature of nonbonding orbital results in an effective attraction on the additional electron to the major sublattice. In addition to the attraction toward the sublattice A, the extra electron from the N dopant is also attracted by the Coulomb interaction of N^+ after N doping. When the N dopant lies at sublattice B, these two attractions are competitive. According to our calculation, the extra electron from the N dopant transfers to sublattice A and occupies an unoccupied nonbonding orbital near the Fermi level, which indicates that the attraction from NBSs is dominant. Hence, the remaining isolated N^+ has a strong ability to attract negative electrons of its neighborhood, which can introduce the impurity energy level above the Fermi level, very similar to the acceptor. On the other hand, when the N dopant lies at sublattice A, the Coulomb interaction will attract the electron toward the doping position and finally results in a localized electronic state around the N dopant with a lower energy. It is worthy noting that, for $n = 6$ GQD, two NBSs are extended and three NBSs are localized at the zigzag edge, which leads to heterogeneous NBSs. The distribution of NBSs near the zigzag edges is slightly denser than that in the inner area, as shown in Figure 7, which also can be obtained from the spin density difference in Figure 3. It is the distance between the N dopant and the edge that determines the energy of impurity level, *viz.*, the degree of localized for impurity states. When the N dopant lies in the sublattice A, with decreasing distance between the N dopant and the edge, the extra electron tends to be tightly restricted around N^+. Consequently, the energies of impurity levels for N-Ax ($x = 3-5$) are lower than those for N-Ax ($x = 0-2$), and they locate far away from the Fermi level. In contrast, for N doped in the sublattice B, with increasing distance between the N dopant and the edge, the ability of N^+ to attract electrons of its neighboring C atoms becomes strong, which causes the impurity energy level of N-Bx ($x = 0-2$) to be more near the Fermi level than N-Bx ($x = 3-5$). In fact, the NBSs localized near the edges are also not homogeneous, namely, the middle of the zigzag edge having a relatively large distribution of NBSs, which can slightly affect the energy of impurity states.

In addition, for N-A1, N-A2, and N-Am cases, as shown in Figure 7, except for occupied NBSs composing impurity states, other occupied NBSs marked by black circles (arrows) are not perfectly distributed exclusively in sublattice A, which is caused by the impurity perturbation. The impurity states of these cases originating from NBSs are localized weakly and lie in the vicinity of other NBSs, which can be characterized by the resonance states. Hence, their corresponding impurity levels are scattered in comparison with sharp impurity levels of other cases.

The electronic structures of B-doped GQD with edge size $n = 6$ have also been investigated. The calculations show that their electronic structures are contrary to those of N-doped $n = 6$ GQD. For B-doped GQDs, the B dopant injects a positive hole into GQDs, and the Fermi level will shift downward slightly. The positive hole induced by the B dopant will reside in the occupied nonbonding orbital of pristine GQDs, and some are exhibited in Figure 8 (see Supporting Information for others). For the fully polarized state $S = 2$ cases, *viz.*, B-Am, B-B0, and B-B3, the added hole simply occupies one spin-up orbital (two degenerate spin-up orbitals are half-filled for B-B0) and other orbitals remain in their spin. However, for other cases, the added hole induces present chargers to be partially flipped in spin, which leads to a greatly modified electronic structure. In contrast to N-doped GQDs, when B dopants lie in the sublattice A, the impurity levels designated by dashed blue arrows (circles) appear above the Fermi level. For GQDs with B doped in the sublattice B, the impurity levels exist below the Fermi level. The formation mechanism of these impurity levels is similar to N doping, which is related to the competition between the following two factors for an extra hole. One is its Coulomb interaction with B^-, and another is its correlation with NBSs. Noting that NBSs have two parts, one is extended in the GQD and the other distributes mainly near the edge. In addition, the electronic states associated with the impurity level are localized around the B dopant and exhibit bonding states along the B−C bonds, which are in accordance with the theoretically and experimently obtained scanning tunneling microscope images.[52−54]

Our present work shows that NBS plays an important role in the electronic properties for both pris-

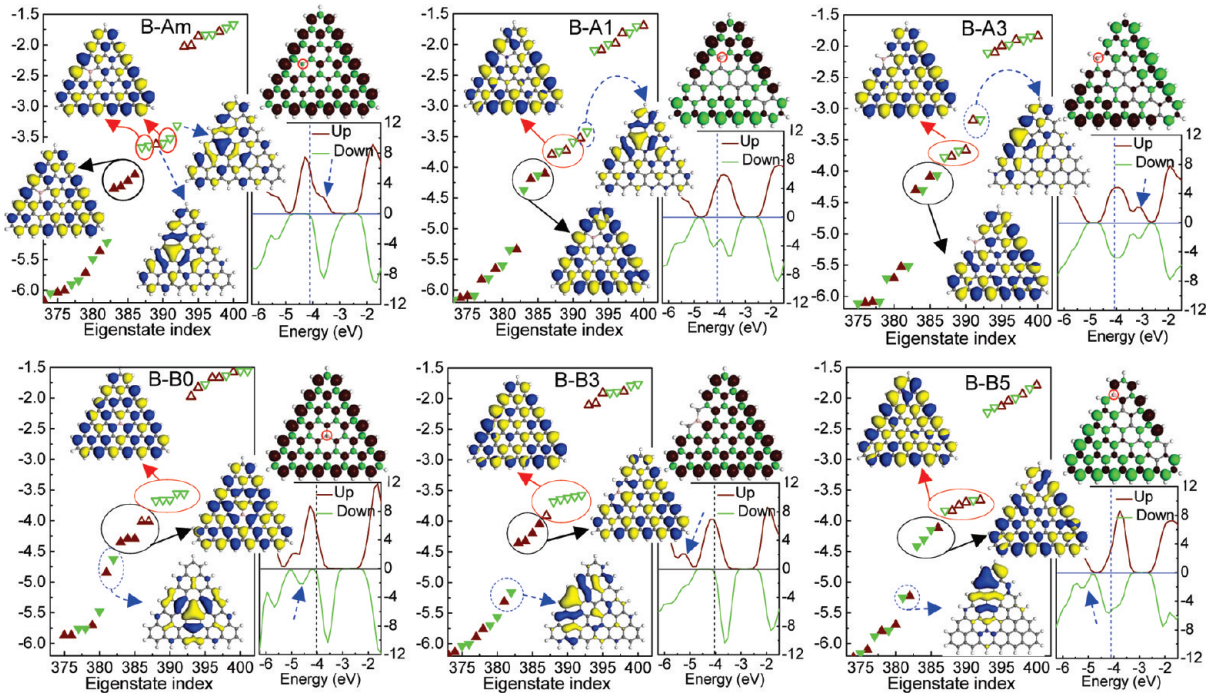

Figure 8. Calculated self-consistent energy spectra, DOS, and isosurfaces of NBSs and spin density difference for B-doped GQDs with size $n = 6$, in which full and empty symbols correspond to full and empty states, respectively. The upward triangle and downward triangle represent up and down spins, respectively. Occupied NBSs and unoccupied NBSs are denoted by black and red circles, respectively.

tine and N/B-doped GQDs, and the interactions between NBS and the impurity atom could be explored based on the electronic structure for N/B-doped GQD. Furthermore, our findings provide one way to control the electronic structure as well as the electronic distribution for triangular GQD with zigzag edges, which is important in designing graphene-based electronic devices.

CONCLUSION

DFT calculations reveal that the triangular-shaped GQD with a zigzag edge exhibits unique electronic properties, in which NBS near the Fermi level originates from the unbalanced sublattice and distributes exclusively at sublattice A. Calculations on N/B-doped GQD show that the total energy and the energy gap depend on both the position and the sublattice of the substitutional N/B atom. The configurations with N/B doped at sublattice A or at the zigzag edge have lower total energies and larger energy gaps. After the N/B doping, the net spin for GQD is reduced and full or partial depolarization occurs, regardless of doping configuration. The N (B) dopant in the sublattice A leads to an impurity state that locates below (above) the Fermi level, while for doping in the sublattice B, an impurity state appears above (below) the Fermi level. We propose that the dependence of the energy level of impurity states on the doping position should be explained by the competition between the Coulomb attraction of N^+ (B^-) and the correlation with charges of NBSs. The sign of the impurity level depends on whether the doping site belongs to the sublattice A or B, and the distance between the N/B dopant and GQD edge decides the energy of impurity level. These results suggest that one way to control the electronic property of GQDs by adjusting N/B doping sites can be realized.

METHODS

In this work, the calculations were carried out using DFT provided by Dmol3 code,[55,56] and the spin-polarized DFT was employed to correctly describe the magnetic moment at the zigzag edge of GQD. In our DFT calculations, the all-electron Kohn−Sham wave functions were expanded in the double numerical polarized atomic orbital basis. The GGA with the Perdew−Burke−Ernzerhof correlation gradient correction was used to describe the exchange and correlation energy.[57] Self-consistent field procedure was done until the change in energy was less than 10^{-6} Hartree, and the geometrical optimization of the structure was done with a convergence criterion of 10^{-5} Hartree on the energy. These calculated conditions allowed us to find the geometric and electronic structure for N/B-doped GQD accurately.

Acknowledgment. The support from National Natural Science Foundation of China (Grant Nos. 50525204, 50832001, and 50902057), the special Ph.D. program (Grant No. 200801830025) from Ministry of Education, Science and Technology Development Programmer of Jilin Province (Grant No. 20090703), Program for Changjiang Scholars and Inovative Research Team in University (PCSIRT), and the "211" and "985" project of Jilin University, China, is highly appreciated.

Supporting Information Available: Other figures of electronic structures of B-doped GQDs. This material is available free of charge *via* the Internet at http://pubs.acs.org.

REFERENCES AND NOTES

1. Novoselov, K. S.; Geim, A. K.; Morozov, S. V.; Jiang, D.; Zhang, Y.; Dubonos, S. V.; Grigorieva, I. V.; Firsov, A. A. Electric Field Effect in Atomically Thin Carbon Films. *Science* **2004**, *306*, 666–669.
2. Novoselov, K. S.; Geim, A. K.; Morozov, S. V.; Jiang, D.; Katsnelson, M. I.; Grigorieva, I. V.; Dubonos, S. V.; Firsov, A. A. Two-Dimensional Gas of Massless Dirac Fermions in Graphene. *Nature* **2005**, *438*, 197–200.
3. Zhang, Y. B.; Tan, Y. W.; Stormer, H. L.; Kim, P. Experimental Observation of the Quantum Hall Effect and Berry's Phase in Graphene. *Nature* **2005**, *438*, 201–204.
4. Bunch, J. S.; Yaish, Y.; Brink, M.; Bolotin, K.; McEuen, P. L. Coulomb Oscillations and Hall Effect in Quasi-2D Graphite Quantum Dots. *Nano Lett.* **2005**, *5*, 287–290.
5. Räder, H. J.; Rouhanipour, A.; Talarico, A. M.; Palermo, V.; Samorì, P.; Müllen, K. Processing of Giant Graphene Molecules by Soft-Landing Mass Spectrometry. *Nat. Mater.* **2006**, *5*, 276–280.
6. Meyer, J. C.; Geim, A. K.; Katsnelson, M. I.; Novoselov, K. S.; Booth, T. J.; Roth, S. The Structure of Suspended Graphene Sheets. *Nature* **2007**, *446*, 60–63.
7. Geim, A. K.; Novoselov, K. S. The Rise of Graphene. *Nat. Mater.* **2007**, *6*, 183–191.
8. Katsnelson, M. I. Graphene: Carbon in Two Dimensions. *Mater. Today* **2007**, *10*, 20–27.
9. Novoselov, K. S.; Jiang, Z.; Zhang, Y.; Morozov, S. V.; Stormer, H. L.; Zeitler, U.; Maan, J. C.; Boebinger, G. S.; Kim, P.; Geim, A. K. Room-Temperature Quantum Hall Effect in Graphene. *Science* **2007**, *315*, 1379.
10. Han, M. Y.; Özyilmaz, B.; Zhang, Y.; Kim, P. Energy Band-Gap Engineering of Graphene Nanoribbons. *Phys. Rev. Lett.* **2007**, *98*, 206805.
11. Özyilmaz, B.; Jarillo-Herrero, P.; Efetov, D.; Abanin, D. A.; Levitov, L. S.; Kim, P. Electronic Transport and Quantum Hall Effect in Bipolar Graphene p−n−p Junctions. *Phys. Rev. Lett.* **2007**, *99*, 166804.
12. Chen, Z. H.; Lin, Y. M.; Rooks, M. J.; Avouris, P. Graphene Nano-ribbon Electronics. *Physica E* **2007**, *40*, 228–232.
13. Vázquez de Parga, A. L.; Calleja, F.; Borca, B.; Passeggi, M. C. G., Jr.; Hinarejos, J. J.; Guinea, F.; Miranda, R. Periodically Rippled Graphene: Growth and Spatially Resolved Electronic Structure. *Phys. Rev. Lett.* **2008**, *100*, 056807.
14. Li, X. L.; Wang, X. R.; Zhang, L.; Lee, S.; Dai, H. J. Chemically Derived, Ultrasmooth Graphene Nanoribbon Semiconductors. *Science* **2008**, *319*, 1229–1232.
15. Wei, D. C.; Liu, Y. Q.; Zhang, H. L.; Huang, L. P.; Wu, B.; Chen, J. Y.; Yu, G. Scalable Synthesis of Few-Layer Graphene Ribbons with Controlled Morphologies by a Template Method and Their Applications in Nanoelectromechanical Switches. *J. Am. Chem. Soc.* **2009**, *131*, 11147–11154.
16. Terrones, M.; Botello-Méndez, A. R.; Campos-Delgado, J. C.; López-Urías, F.; Vega-Cantú, Y. I.; Rodríguez-Macías, F. J.; Elías, A. L.; Muñoz-Sandoval, E.; Cano-Márquez, A. G.; Charlier, J. C.; *et al.* Graphene and Graphite Nanoribbons: Morphology, Properties, Synthesis, Defects and Applications. *Nano Today* **2010**, *5*, 351–372.
17. Rutter, G. M.; Guisinger, N. P.; Grain, J. N.; First, P. N.; Stroscio, J. A. Edge Structure of Epitaxial Graphene Islands. *Phys. Rev. B* **2010**, *81*, 245408.
18. Fujita, M.; Wakabayashi, K.; Nakada, K.; Kusakabe, K. Peculiar Localized State at Zigzag Graphite Edge. *J. Phys. Soc. Jpn.* **1996**, *65*, 1920–1923.
19. Wakabayashi, K.; Fujita, M.; Ajiki, H.; Sigrist, M. Electronic and Magnetic Properties of Nanographite Ribbons. *Phys. Rev. B* **1999**, *59*, 8271–8282.
20. Ezawa, M. Peculiar Width Dependence of the Electronic Properties of Carbon Nanoribbons. *Phys. Rev. B* **2006**, *73*, 045432.
21. Nakada, K.; Fujita, M.; Dresselhaus, G.; Dresslhaus, M. S. Edge State in Graphene Ribbons: Nanometer Size Effect and Edge Shape Dependence. *Phys. Rev. B* **1996**, *54*, 17954–17961.
22. Yu, S. S.; Wen, Q. B.; Zheng, W. T.; Jiang, Q. Electronic Properties of Graphene Nanoribbons with Armchair-Shaped Edges. *Mol. Simulat.* **2008**, *34*, 1085–1090.
23. Son, Y. W.; Cohen, M. L.; Louie, S. G. Energy Gaps in Graphene Nanoribbons. *Phys. Rev. Lett.* **2006**, *97*, 216803.
24. Son, Y. W.; Cohen, M. L.; Louie, S. G. Half-Metallic Graphene Nanoribbons. *Nature* **2006**, *444*, 347–349.
25. Sun, C. Q.; Fu, S. Y.; Nie, Y. G. Dominance of the Broken Bonds and the Unpaired Nonbonding Electrons in the Band Gap Expansion and the Edge States Generation in Graphene Nanoribbons. *J. Phys. Chem. C* **2008**, *112*, 18927–18934.
26. Shemella, P.; Zhang, Y. M.; Mailman, M.; Ajayan, P. M.; Nayak, S. K. Energy Gaps in Zero-Dimensional Graphene Nanoribbons. *Appl. Phys. Lett.* **2007**, *91*, 042101.
27. Hod, O.; Peralta, J. E.; Scuseria, G. E. Edge Effects in Finite Elongated Graphene Nanoribbons. *Phys. Rev. B* **2007**, *76*, 233401.
28. Hod, O.; Barone, V; Scuseria, G. E. Half-Metallic Graphene Nanodots: A Comprehensive First-Principles Theoretical Studty. *Phys. Rev. B* **2008**, *77*, 035411.
29. Ezawa, M. Metallic Graphene Nanodisks: Electronic and Magnetic Properties. *Phys. Rev. B* **2007**, *76*, 245415.
30. Fernández-Rossier, J.; Palacios, J. J. Magnetism in Graphene Nanoislands. *Phys. Rev. Lett.* **2007**, *99*, 177204.
31. Wang, W. L.; Meng, S.; Kaxiras, E. Graphene NanoFlakes with Large Spin. *Nano Lett.* **2008**, *8*, 241–245.
32. Ezawa, M. Coulomb Blockade in Graphene Nanodisks. *Phys. Rev. B* **2008**, *77*, 155411.
33. Güclü, A. D.; Potasz, P.; Voznyy, O.; Korkusinski, M.; Hawrylak, P. Magnetism and Correlations in Fractionally Filled Degenerate Shells of Graphene Quantum Dots. *Phys. Rev. Lett.* **2009**, *103*, 246805.
34. Potasz, P.; Güclü, A. D.; Hawrylak, P. Zero-Energy States in Triangular and Trapezoidal Graphene Structures. *Phys. Rev. B* **2010**, *81*, 033403.
35. Kuc, A.; Heine, T. Structural and Electronic Properties of Graphene Nanoflakes. *Phys. Rev. B* **2010**, *81*, 085430.
36. Lieb, E. H. Two Theorems on the Hubbard Modal. *Phys. Rev. Lett.* **1989**, *62*, 1201–1204.
37. Singh, A. K.; Penev, E. S.; Yakobson, B. I. Vacancy Clusters in Graphene as Quantum Dots. *ACS Nano* **2010**, *4*, 3510–3514.
38. Wang, W. L.; Yazyev, O. V.; Meng, S.; Kaxiras, E. Topological Frustration in Graphene Nanoflakes: Magnetic Order and Spin Logic Devices. *Phys. Rev. Lett.* **2009**, *102*, 157201.
39. Recher, P.; Trauzettel, B. Quantum Dots and Spin Qubits in Graphene. *Nanotechnology* **2010**, *21*, 302001.
40. Golberg, D.; Bando, Y.; Han, W.; Kurashima, K.; Sato, T. Single-Walled B-Doped Carbon, B/N-Doped Carbon and BN Nanotubes Synthesized from Single-Walled Carbon Nanotubes through a Substitution Reaction. *Chem. Phys. Lett.* **1999**, *308*, 337–342.
41. Czerw, R.; Terrones, M.; Charlier, J.-C.; Blasé, X.; Foley, B.; Kamalakaran, R.; Grobert, N.; Terrones, H.; Tekleab, D.; Ajayan, P. M.; *et al.* Identification of Electron Donor States in N-Doped Carbon Nanotubes. *Nano lett.* **2001**, *1*, 457–460.
42. Manaa, M. R.; Sprehn, D. W.; Ichord, H. A. Prediction of Extended Aromaticit for a Novel $C_{48}N_{12}$ Azafullerene Structure. *J. Am. Chem. Soc.* **2002**, *124*, 13990–13991.
43. Li, L. J.; Glerup, M.; Khlobystov, A. N.; Wiltshire, J. G.; Sauvajol, J. L.; Tavlor, R. A.; Nicholas, R. J. The Effects of Nitrogen and Boron Doping on the Optical Emission and Diameters of Single-Walled Carbon Nanotubes. *Carbon* **2006**, *44*, 2752–2757.
44. Wei, D. C.; Liu, Y. Q.; Wang, Y.; Zhang, H. L.; Huang, L. P.; Yu, G. Synthesis of N-Doped Graphene by Chemical Vapor Deposition and Its Electrical Properties. *Nano Lett.* **2009**, *9*, 1752–1758.

45. Handuja, S.; Srivastava, P.; Vankar, V. D. Structural Modification in Carbon Nanotubes by Boron Incorporation. *Nanoscale Res. Lett.* **2009**, *4*, 789–793.
46. Wang, X. R.; Li, X. L.; Zhang, L.; Yoon, Y.; Weber, P. K.; Wang, H. L.; Guo, J.; Dai, H. J. N-Doping of Graphene through Electrothermal Reactions with Ammonia. *Science* **2009**, *324*, 768–771.
47. Kitchen, D.; Richardella, A.; Tang, J. M.; Flatte, M. E.; Yazdani, A. Atom-by-Atom Substitution of Mn in GaAs and Visualization of Their Hole-Mediated Interactions. *Nature* **2006**, *442*, 436–439.
48. Zheng, W. T.; Sun, C. Q. Electronic Process of Nitriding: Mechanism and Applications. *Prog. Solid State Chem.* **2006**, *34*, 1–20.
49. Yu, S. S.; Zheng, W. T. Effect of N/B Doping On the Electronic and Field Emission Properties for Carbon Nanotubes, Carbon Nanocones, and Graphene Nanoribbons. *Nanoscale* **2010**, *2*, 1069–1082.
50. Ayala, P.; Rubio, A.; Pichler, T. The Physical and Chemical Properties of Heteronanotubes. *Rev. Mod. Phys.* **2010**, *82*, 1843–1885.
51. Yu, S. S.; Zheng, W. T.; Wen, Q. B.; Jiang, Q. First Principle Calculations of the Electronic Properties of Nitrogen-Doped Carbon Nanoribbons with Zigzag Edges. *Carbon* **2008**, *46*, 537–543.
52. Yu, S. S.; Zheng, W. T.; Jiang, Q. Electronic Properties of Nitrogen-/Boron-Doped Graphene Nanoribbons with Armchair Edges. *IEEE Trans. Nanotechnol.* **2010**, *9*, 78–81.
53. Endo, M.; Hayashi, T.; Hong, S. H.; Enoki, T.; Dresselhaus, M. S. Scanning Tunneling Microscope Study of Boron-Doped Highly Oriented Pyrolytic Graphite. *J. Appl. Phys.* **2001**, *90*, 5670–5674.
54. Miwa, R. H.; Martins, T. B.; Fazzio, A. Hydrogen Adsorption on Boron Doped Graphene: An *Ab Initio* Study. *Nanotechnology* **2008**, *19*, 155708.
55. Delley, B. An All-Electron Numerical Method for Solving the Local Density Functional for Polyatomic Molecules. *J. Chem. Phys.* **1990**, *92*, 508–517.
56. Delley, B. From Molecules to Solids with the DMol(3) Approach. *J. Chem. Phys.* **2000**, *113*, 7756–7764.
57. Perdew, J. P.; Burke, K.; Ernzerhof, M. Generalized Gradient Approximation Made Simple. *Phys. Rev. Lett.* **1996**, *77*, 3865–3868.